A detailed simulation of F_2 measurability at HERA

G.Bernardi[1] , W. Hildesheim
Laboratoire de Physique Nucléaire et de Hautes Energies
Paris, France

Abstract

A study on the measurement of the F_2 proton structure function is presented, based on a realistic montecarlo of the H1 detector. The influence of systematic errors and detector acceptance on the values of x, y and Q^2 was studied in four independent reconstruction methods, based on: the electron only, the hadrons only, or 2 separate combinations of electronic and hadronic information.In particular, results from the combined measurement of y with the hadronic system, and Q^2 from the electron indicate that the evolution of F_2 will be measurable at low Q^2 ($\sim 50GeV^2$) on two orders of magnitude in x.

1 Introduction

Structure function measurements have the characteristics to be, among other things, fundamental but painful to achieve. In this report we will, unfortunately for the reader, concentrate on the second but necessary aspect, if we except the next few sentences.

The structure function program at HERA is very complete, covering charged and neutral currents (NC) over unknown kinematical areas at the highest and lowest x and Q^2 ever achieved. However the domain that can be explored is completely disconnected (until HERA is ran at lower energies) from the present "fixed target" measurements, rendering the experimental task more difficult. Here, we try to see if we will be able to bridge the gap with the previous results, by combining measurements on the electron and on the hadronic flow. In the first months of data taking, the attention will especially focus on the F_2 structure function at low x, (and thus low Q^2), whose behaviour is largely a matter of speculation at present[2]. The numerous structure function parametrizations which agree on the existing data, show large discrepancies as soon as we move to the low x region. The theoretical interpretation is also unclear at present, and the constraint brought by the data will at least allow a better understanding of the transition between the perturbative and non-pertubative QCD regime, and at best unveil signs of new physics. From the experimental point of view, very early enough statistics will be available, whatever the machine conditions will be, which does not mean that results will be available right away, since a high precision is always required in this kind of measurement. Among the important sources of uncertainty are the knowledge of the absolute luminosity, and the absolute energy calibration of the detectors. In the beginning, the error made on the F_2 measurement at a given point (up to 50% when combining several effects), will prevent from knowing the F_2 behaviour, if we do

[1]present address: DESY, Notkestrasse 85, D-2000 Hamburg 52, Germany
[2]see J.Bartels/J.Feltesse report on low x physics in these proceedings

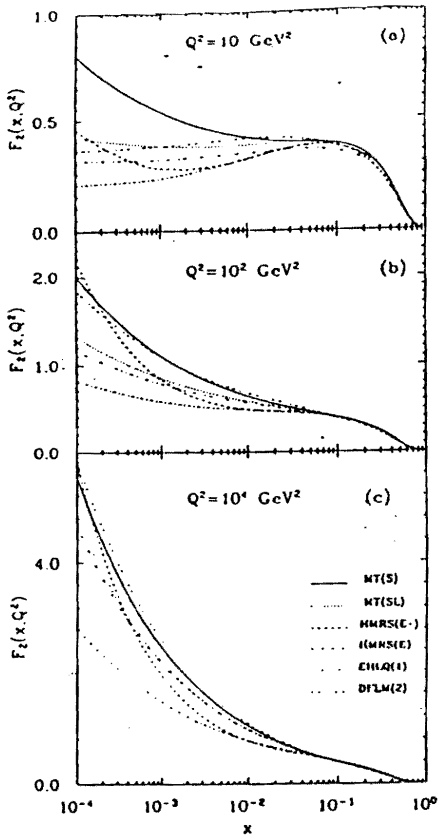

Fig.1

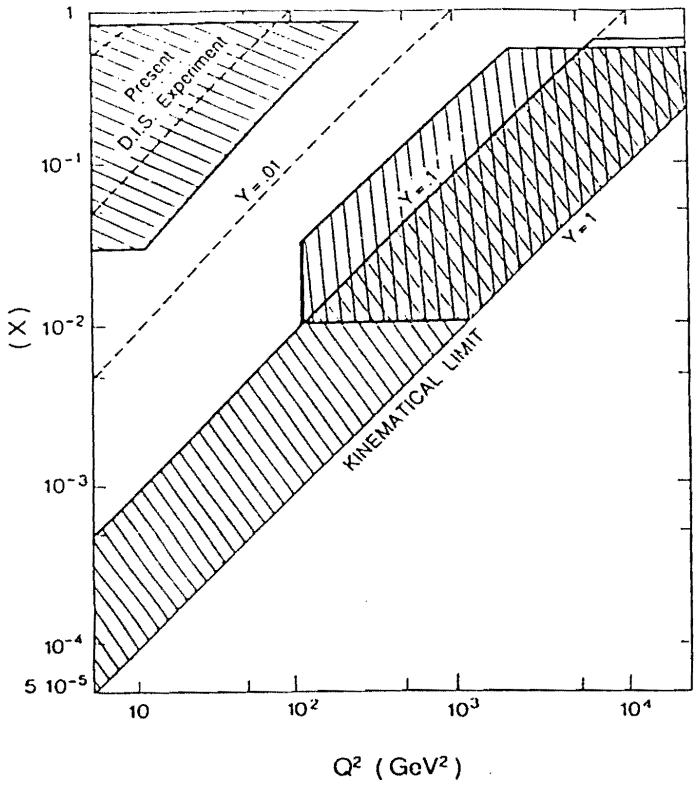

Fig.2

Domains where systematic errors are below 10% for :

: electron measurement

: hadron flow measurement

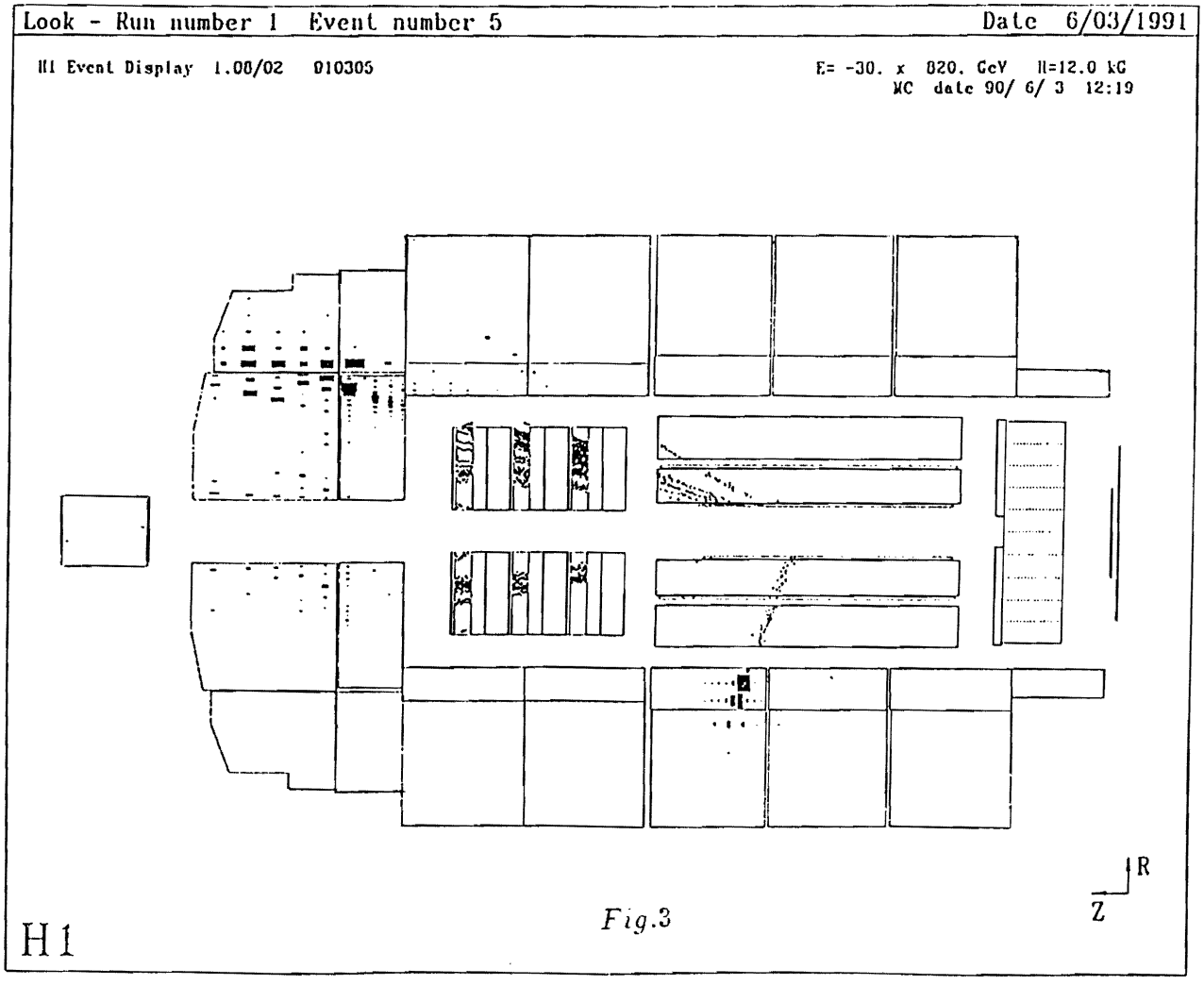

Fig.3

not also rely on its evolution along x at a given Q^2. Fig.1, extracted from [1], shows for instance some F_2 predicted behaviours at three different Q^2, which might be separated by studying their relative evolution if the lever arm along x is large enough. The discrimination is best done at low Q^2 ($\leq 300GeV^2$), which is a region where the structure function F_2[3] is related in a simple way to the cross-section since the interaction happens dominantly through photon exchange:

$$\frac{d\sigma^2}{dx\ dQ^2} = \frac{2\pi\alpha^2}{xQ^4}\ [1+(1-y)^2]\ F_2(x,Q^2)$$

Here, for simplification, we also considered that the Callan-Gross relation holds rendering the ratio R=σ_L/σ_T to be equal to 0, which is only a rough estimation at very low x. In Fig.2 we see the kinematical region explored by the precedent experiments and the new region expected to be measurable at *HERA* according to the *HERA* 87 workshop [2]. At low Q^2 the simpler and most precise cross-section measurement available is obtained via the angle and energy of the electron, but it is reliable on only roughly one order of magnitude in x at a given Q^2. One of the main goal of this study has been to try to extend the lever arm in x by making use of the information from the electron and from the hadrons at the same time.

To be conclusive on this point we had to study with a detailed simulation the reconstruction of x and Q^2 in the H1 detector, taking into account the main experimental effects: granularity, acceptance, energy and angular resolutions, biases and miscalibrations. At the same time a large montecarlo statistics and a high precision are needed and the procedure might have to be iterated for every new effect to be studied. We present in the next section how we coped with this simulation, in order to obtain precise results in a reasonable time.

We did not study the influence of different input structure functions on the acceptance, since this effect has been treated elsewhere [2] [3] and can be removed in an iterative unfolding procedure. No radiative effects were included in the studied event samples, although we briefly discuss a possible treatment of these events in the last section[4]. We have not simulated either, trigger and background effects. The first one because the neutral and charged currents studied here after do not exhibit big triggering problems, the second one because they are studied in separate reports, and are believed to be removable after analysis (except maybe in the very high y region).

We will present in section 2 the analysis chain used, insisting on the original content of the simulation part. In section 3 we will study the cross-sections of neutral and charged currents obtained with hadronic system only, while section 4 will deal with NC measurement based on the electron alone. Section 5 will compare the two most popular methods of combination of electron and hadrons information, and show the improvements obtained. In conclusion we will mention the areas which still deserve urgent study.

[3]The kinematics of deep inelastic scattering is fixed by a set of two variables, and we chose in this study the usual momentum transfer Q^2 and Bjorken x. We then have $F_2 = F_2(x,Q^2)$.

[4]see the "radiative correction" part of these proceedings for more details.

2 Analysis chain description

The analysis chain relied mostly on standard H1 programs, or on developments which entered afterwards in the H1 libraries. This study thus shows what can be achieved within a few months of the start of the experiment. The chain has been performed in 4 steps, on the IBM-3090 of the IN2P3 computer center in Lyon:

- d.i.s. event generation.
- detailed simulation inside the H1 detector with the "calibrated" option".
- reconstruction of the simulated event.
- analysis and display of the reconstructed quantities.

2.1 Event generation

Two classes of events were generated with LEPTO 5.2 with default parameters and parton shower option:
- 3000 charged currents, with EHLQ1 parametrisation, between 10 and $10^5 GeV^2$ in Q^2, according to cross-sections inside a grid binned with 2 bins per order of magnitude in x and Q^2.
- 18000 neutral currents, with MT-B2 parametrisation, between 3 and $10^5 GeV^2$ in Q^2, according to cross-sections inside a grid binned with 4 bins per order of magnitude in x and Q^2.

We chose the extreme MT-B2 parametrisation since it is the most atypical one (it displays the fastest cross-section variations at low Q^2) thus implying a severe test of the "unfolding" procedure.

2.2 Detailed simulation/reconstruction inside the H1 detector

By saying "detailed" we mean that the geometry was described in the GEANT framework, although we did not use the most detailed geometry description available. The homogeneous active parts of the calorimeter were averaged, while the inhomogeneous dead material regions where unwanted "tails" appear were described in detail. The electromagnetic showers (including those originating in hadronic showers) were parametrized in the homogeneous regions, but tracked in detail in the dead regions. Hadronic interactions were simulated with GHEISHA, and the resulting hadrons were always tracked in detail but "terminators" where applied to proton and neutrons when their kinetic energy was smaller than a low threshold. Finally, the average cpu-time used for a neutral current event was around 30", and its output size around 100 kbytes. An example of a simulated high Q^2 neutral current is shown in Fig.3. The electron (towards the bottom of the picture), the current jet, and the remnants of the target jet in the very forward direction (left of the picture) are clearly visible.

The main difference between the ZEUS and the H1 calorimeter is that the H1 device is non-compensating, i.e. the electromagnetic and the hadronic response are different. However, off-line "π^0 weighting" techniques can restore the equality of responses and renders the energy resolution gaussian [4]. This technique will be applied to the data.

Nevertheless for the montecarlo events an alternative has been devised to avoid the long job of determination of the "weighting" parameters for the montecarlo: the so-called "calibrated option" [5] that will now be briefly described.

The "calibrated option" performs the calorimeter simulation in two independent steps. The first one and by far the most cpu-time-consuming, follows the development of the shower and log the deposition of all the energy (including the "invisible" energy lost in nuclear break-ups or in escaping particles (ν,...)) in the active cells or in any other dead area. At this point the energy conservation is perfect. In the second step we are able:
- either to reproduce the visible energy as it will appear in our data, by "killing" the invisible energy and by applying the sampling fluctuations which produce the energy resolutions characteristic of our calorimeters.
- or to provide a gaussian response as it will be after "weighting", by making use of the invisible energy: the actual "calibrated" way.
Both options have been extensively tested, and reproduce the results obtained in the conventional way, were the sampling fluctuations are not disentangled from the shower development. It should be stressed that the results obtained in the "calibrated" option are not at all comparable with a simple 4-vector smearing: in our option the response is gaussian only in homogeneous parts of the calorimeter, and "tails" arise "naturally" from the dead material corrections which are applied when the showers cross a crack. All these corrections are performed as they will be for the real data. The granularity and the dead areas are also described with high precision. Finally, the development of the shower being exactly simulated, the "edge" effects, like particle losses in the beam pipe or in cracks are as realistic as a detailed montecarlo can be, and the particle identification efficiency can be estimated by applying the same algorithms which will be applied to data.

2.3 Detector response

We used in this simulation the calorimetric characteristics of the H1 detector,which varies with the polar angle θ ($\theta = 0^0$ is the proton direction). For the hadronic response, we encounter successively, starting from the very forward region:

$0.6^0 \leq \theta \leq 4^0$	: plug calorimeter:	$\sigma(E_h)/E_h = 100\%/\sqrt{E_h}$
$4.0^0 \leq \theta \leq 135^0$	: Liquid argon calorimeter:	$\sigma(E_h)/E_h = 50\%/\sqrt{E_h}$
$135^0 \leq \theta \leq 176^0$	: backward electromagnetic calorimeter (BEMC), no standalone hadronic measurement ($\sim 1\lambda$).	

These last 2 calorimeters are backed up by an Iron tail-catcher of 3 to 4 λ, which has an approximate hadronic resolution $\sigma(E_h)/E_h \sim 100\%/\sqrt{E_h}$

for the electromagnetic showers:

$\sigma(E)/E = 13\%/\sqrt{E} \oplus 1\%$ in the liquid argon.
$\sigma(E)/E = 10\%/\sqrt{E} \oplus 1\%$ in the BEMC.

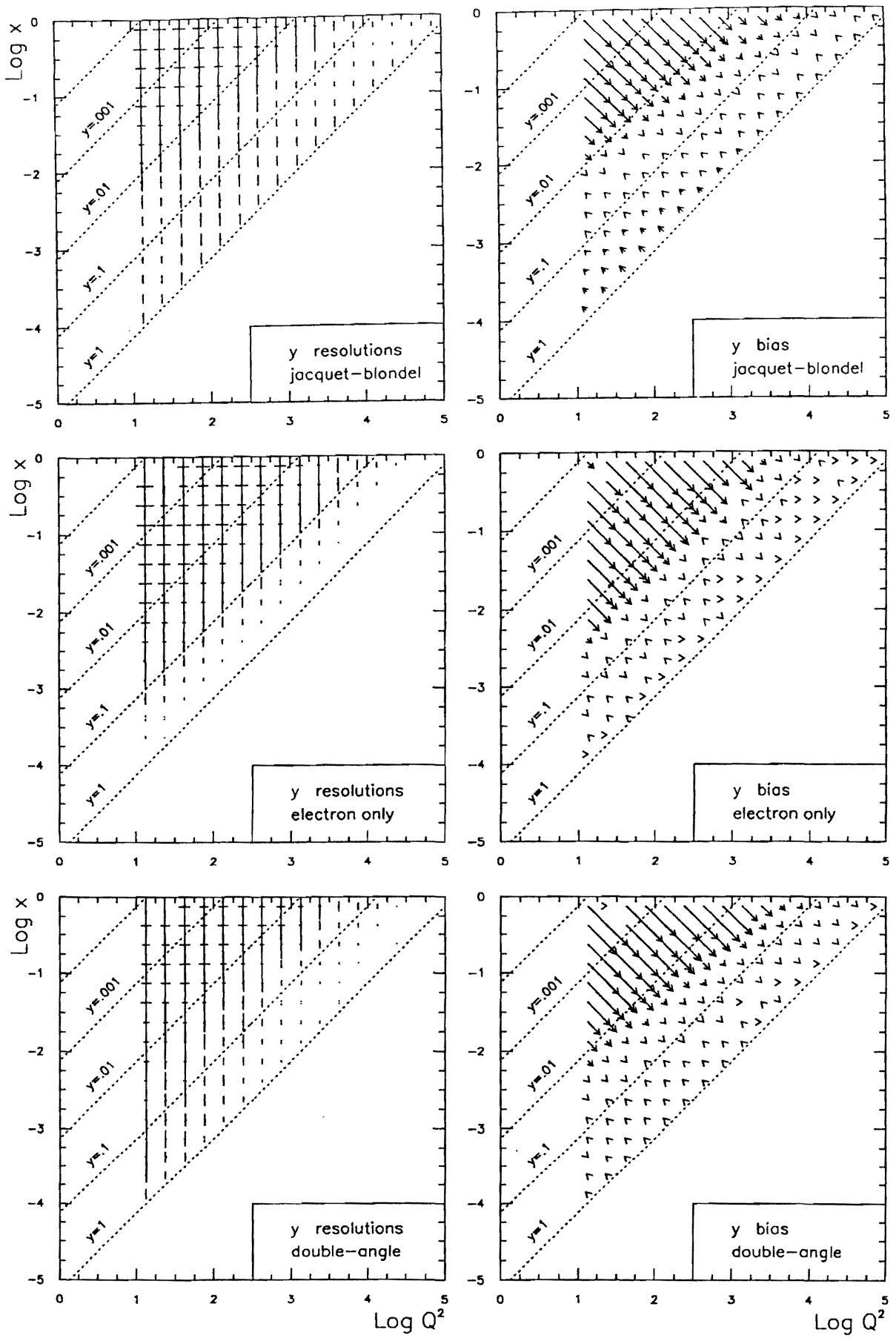

Figure 4 a b c d e f

In the resolutions plots, the vertical error bars display the resolutions of $\Delta y/y$:
A bar which is one graduation interval long represents a resolution of 25 % .
In the plot of the biases, the arrows are drawn between the center of a bin, and the mean value of y reconstructed in this bin.

The following results can be roughly transferred to the ZEUS configuration if manipulated with some care due to the main generic[5] calorimetric differences:

- The ZEUS calorimeter has a better hadronic coverage (especially in the backward region), and a better (compensated) hadronic resolution, but a coarser granularity.
- It has also a much coarser granularity for e^- and photons, and a poorer energy resolution than H1 electromagnetic calorimeters.

3 Cross-section measurement: hadrons only

Charged current events will be produced at a much lower rate than neutral current events, and in fact for the first pb^{-1} only around 60 are expected, but it is a good exercise to foresee what will happen with a reasonable statistics (say $100pb^{-1}$), since in the CC case only hadrons are available for determining the kinematical variables.

3.1 The Jacquet-Blondel method

A model-independent method to determine x and Q^2, has been proposed by A.Blondel and F.Jacquet [6] in an early ep workshop and is based on kinematics only:

p_{xh}, p_{yh}, p_{zh} being the three momentum components of a hadron and E_e, E_p the incident energy of the electron and proton, we obtain by summing on all hadrons:

$$y = \frac{\sum_h (E_h - p_{zh})}{2E_e}$$

$$Q^2 = \frac{(\sum_h p_{xh})^2 + (\sum_h p_{yh})^2}{1-y}$$

$$x = \frac{Q^2}{s\ y} \qquad s = 4E_eE_p$$

Each hadron produced at the vertex contributes to y by $\sin^2(\gamma/2).E_h/E_e$, where γ is the polar angle of the hadron, and E_e the incident energy of the electron. The contributions of the hadrons close to the beam pipe (γ small) increase as γ^2 (for a given energy), thus largely diminishing the influence of particle losses in the beam pipe. This also causes a subtle but important experimental effect that we will call the "granularity" effect (refering to the granularity, i.e. the cell density, of the calorimeter): By applying the Jacquet-Blondel method to the cell centroids, we bias γ and thus y towards larger values, and it is shown in Fig.4b that this effect, if not corrected, beats the opposite effect due to particle losses in the beam pipe. Both these effects effectively influence the y determination only when the current jet is approaching the forward direction ($\gamma \sim 10^0$ i.e. $y \sim 0.01$ at low Q^2). The "granularity" effect is in fact the combination of two different biases :

- When computing y from calorimetric information, we put all the energy of a cell in its center of gravity. However the contribution of a particle to y is "weighted" by $sin^2\gamma/2$,

[5] No attempt is made here to compare the delicate procedure of calibration of these detectors or the spatial distribution of their "cracks".

and *in average*, the mean γ which results from integrating $\sin^2\gamma/2$ along a cell (assuming a uniform energy density inside the cell) is greater than the γ obtained with the center of gravity. In a fine-grained calorimeter like in H1, this effect can be neglected. The bias brought on y ,considering only this particle, is[6]:

$$\frac{y_{rec} - y_{true}}{y_{true}} = -\frac{\phi^2}{3\gamma^2}$$

where ϕ is the angular granularity, and $\phi = 1^0$ in the H1 forward hadronic calorimeter. Thus for angles greater than 6^0, the bias is less than -1%. We can remark that this bias which is purely geometrical becomes very large for coarse granularities.
- The energy of a particle undergoes in a calorimeter an angular dispersion, while it is "showering". This effect is dependent on the calorimeter and particle type, and thus very difficult to correct for. Furthermore it becomes very important when approaching the beam pipe as we can see here in a simple example:

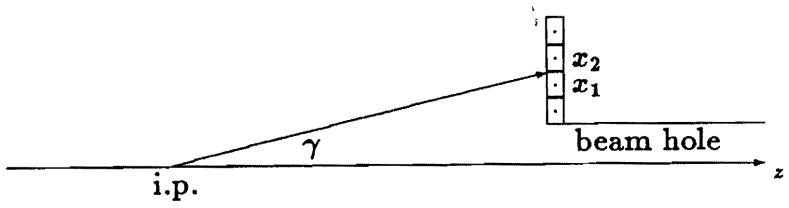

The particle hits the calorimeter and let us assume that its energy goes half in cell x_1, and half in cell x_2. We can compute the contribution to y in this configuration with respect to the true y: we obtain, using $\sin\gamma \sim \gamma$,

$$\frac{y_{rec} - y_{true}}{y_{true}} = \frac{(x_2 - x_1)^2}{(x_2 + x_1)^2}$$

where x_2 and x_1 can be expressed in any units, like angles for instance. Then $x_2 + x_1 = 2\gamma$, and $x_2 - x_1 = \phi$. If the shower now extends on $2n$ cells the bias becomes assuming uniform energy sharing:

$$\frac{1}{n}[\phi^2/4\gamma^2 + (3\phi)^2/4\gamma^2] + \ \dots \ + ((2n-1)\phi)^2/4\gamma^2] \ = \ \frac{\phi^2}{3\gamma^2}\,(n^2 - \frac{1}{4})$$

thus quadratically increasing with the spatial extension of the shower. As an example, assuming a "pencil" current jet at 7^0 whose showers extends transversally on 8 cells ($\phi = 1^0$) we obtain a bias on y of $+11\%$! which explains qualitatively the situation observed in Fig.4b. A coarser granularity would give even worst results, since in average it makes the shower appearing "bigger" than it is, however the previous purely geometrical effect cannot be neglected anymore in this case, and the $(n^2 - \frac{1}{4})$ term becomes $(n^2 - \frac{5}{4})$. A possible way out would be to use the angle of the axis of the showers, if we were able to have a one-to-one relation between showers and particles, but this is difficult to achieve in the forward region. If we take the axis of a "jet", then we put an additional bias on y by averaging the different angles of several particles. We can conclude that having a fine granularity is an important advantage for the measurement of events with "jets" close to the beam pipe, and that correcting for the "granularity" effect is very difficult once we fold in the variations of the energy densities inside the showers.

[6]The formulas on the "granularity" are valid for angles not too large ($\gamma \leq 30^0$).

Let us also remark that when the current jet points towards the "backward" region, i.e. for $\gamma > 140^0$, the angle factor is always between .9 and 1. and thus y is essentially determined by the precision of the hadronic energy response, and practically independent from the angular determination The imperfect hadronic coverage in the "backward" region in H1 is displayed in Fig.4b, where non-negligible negative y biases are visible for $y \geq 0.5$ and $Q^2 \leq 1000 GeV^2$.

Another dangerous source of mismeasurement of y is the presence of calorimetric "pile-up" , especially in the backward area. The presence of only $300 MeV$ of noise in this backward area already produces a shift of 0.01 in y, thus all the efforts to extend the F_2 measurement will be spoiled if these effects could not be corrected [7].

Nevertheless, in the y band between 0.1 and 0.01 which we want to explore, the smallest bias and the better resolutions are achieved when using the Jacquet-Blondel method, as can be seen in comparison with 2 other methods described later on, ("electron-only" and "double-angle"), in Fig.4 . These 2 methods are better for $y > 0.1$ but the J.-B. method is still acceptable there, allowing cross-checks.

The Q^2 determination is much less precise, since it involves $\vec{P}_\perp^2$ which is severely influenced by particle losses in the beam pipe. Neglecting the effect of angular precision, we have in terms of resolution:

$$\frac{\delta Q^2}{Q^2_{true}} = \frac{2-y}{1-y}\frac{\delta E_{jet}}{E_{jet}} \qquad (\delta A \ means \ A_{obs} - A_{true})$$

Thus at low y, the losses in the beam pipe increase, degrading the Q^2 determination, and at higher y, the $(2-y)/(1-y)$ term increases rapidly, spoiling the precision of the measurement. These analytical predictions are confirmed by the results of our montecarlo, presented in Fig.5a,b. It appears from the Fig.5a that a binning of 2 bins per order of magnitude (instead of 4) would be more adapted when measuring x and Q^2 with the J.-B. method, if we want to keep inside a given bin a reasonable fraction of its original content.

3.2 Cross-section measurability in the (x, Q^2) plane

In order to define the conditions to be fulfilled by the "measurable" area we have first to introduce, with the same terminology than [2], the concept of "smeared acceptance". The cross-sections are measured bin by bin in the (x, Q^2) plane, but event migrations occur between the bins due to measurement errors. To obtain the true cross-section in a given bin we have to divide the observed(reconstructed) cross-section by a discontinuous function, the "smeared acceptance" function $A(x, Q^2)$ which depends strongly on the choosed binning, and not only on the cross-sections and on the detector acceptance. We define:

$$\sigma_{true}(x, Q^2) = \sigma_{obs}(x, Q^2)/A(x, Q^2)$$

where $A(x, Q^2)$ takes into account all the migrations, in and out, of the (x, Q^2) bin. We also define the "genuine-fraction" function $GF(x, Q^2)$, as the fraction of observed events in a bin which originated in this bin. Note that this number depends also on the fraction of events which have migrated into the bin under consideration.

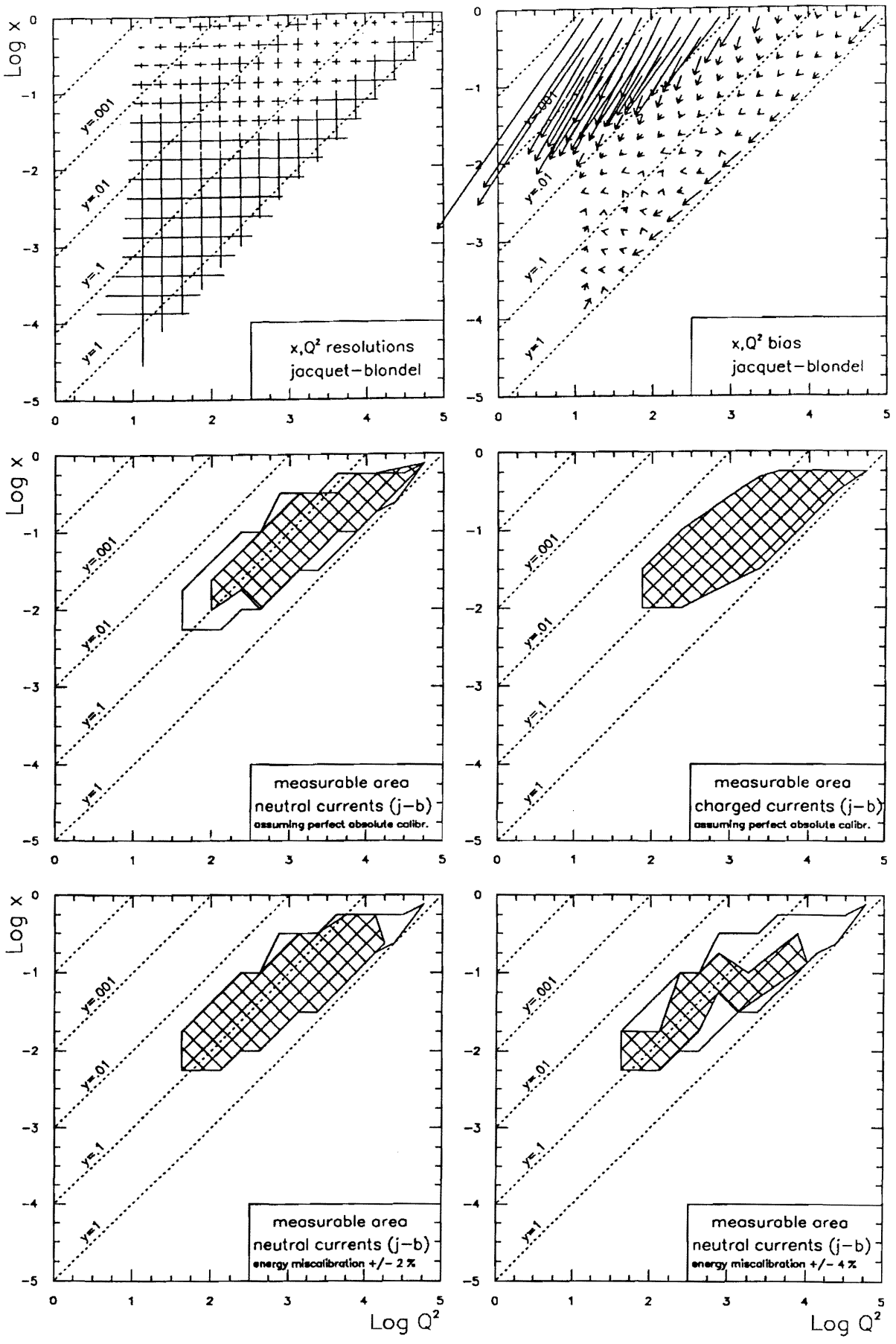

Figure 5 a b c d e f (See Fig.8 for explanations of Fig.5a,b)

The largest contour is always the area obtained with the weak smearing condition and no systematics.
In Fig.5c,d the hatched areas are obtained with the strong smearing condition and no systematics.
In Fig.5e,f the hatched regions are the measurable areas taking into account the systematic errors.

At this point some common sense restrictions must be put on the values of $A(x,Q^2)$ and $GF(x,Q^2)$ of a bin that we still want to call measurable. We will consider two cases, called hereafter the strong and weak acceptance condition:

$$0.75 \leq A(x,Q^2) \leq 1.25 \qquad and \qquad GF(x,Q^2) \geq 0.50$$
$$0.50 \leq A(x,Q^2) \leq 1.50 \qquad and \qquad GF(x,Q^2) \geq 0.40$$

The first case is very safe, while the second is about the limit that previous d.i.s. experiments used to accept. They will both help in showing the variability of the measurable area when going from one set of conditions to the other.
The previous conditions define an initial region of which the "measurable" area is a subset wherein the smeared acceptance function is stable against systematic errors: $A(x,Q^2)$ is stable in the bin (x,Q^2) if $\Delta A(x,Q^2) \leq 10\%$, (i.e. the cross-section will be known within $\pm 10\%$), for a given set of systematic error variations.The "measurable" areas presented in the next figures are obtained from an initial region defined by the weak acceptance condition, except if stated otherwise.

3.3 NC and CC results using the Jacquet-Blondel method

We describe the results obtained only with the hadrons very briefly since CC will not be numerous in the beginning, and NC are much better measured making use of the electron information. In Fig.5c,d we display the measurable areas for NC and CC assuming a perfect absolute calibration and enough luminosity (at least 25 pb^{-1} for the CC when using 2 bins per order of magnitude in x and Q^2). For the charged currents, the results are similar to what was already found in 87 [2] with the exception that the high y band is now excluded. This is clearly understandable when looking at the biases in that region (Fig.5b).
In Fig.5e,f we display the effect of an hadronic energy miscalibration of $\pm 2\%$ and $\pm 4\%$ on the measurable area of the neutral currents. The area shrinks in case of large miscalibrations, especially at high Q^2, and this is true also for charged currents.

4 Cross-section measurement: electron only

In the past twenty-five years, all the d.i.s. experiments have heavily relied on the measurement of the outgoing charged lepton, to obtain the behaviour of the structure functions of the nucleon. At HERA, where the first non-fixed target d.i.s. experiments will soon run, the situation is somewhat different, since the interaction resembles more a collision in the center of mass rather than a "classical" lepton scattering. Nevertheless the advantages of relying mainly on the outgoing electron are still with us, namely its clear-cut signature which eases all the systematic error studies. In the following, after some analytical remarks, we will review the treatment that we applied to the electron, and then draw some conclusions on the measurement that we should be able to achieve in this way.

4.1 Electron reconstruction of x and Q^2

Given:

E_e=incoming electron energy (=30 GeV nominally).

E_p=incoming proton energy (=820 GeV nominally).

θ=angle of the outgoing electron, w.r.t. proton direction. (in the text, scattering angle must be understood as $\pi - \theta$)

E=outgoing electron energy.

The expressions of x and Q^2 are:

$$x = \frac{EE_e \cos^2 \frac{\theta}{2}}{E_p(E_e - E \sin^2 \frac{\theta}{2})}$$

$$y = 1 - \frac{E}{E_e} \sin^2 \frac{\theta}{2}$$

$$Q^2 = 4EE_e \cos^2 \frac{\theta}{2}$$

which by derivation lead to:

$$\frac{dx}{x} = \frac{1}{y}\frac{dE}{E} + \tan\frac{\theta}{2}(x\frac{E_p}{E_e} - 1)d\theta$$

$$\frac{dQ^2}{Q^2} = \frac{dE}{E} - \tan\frac{\theta}{2}d\theta$$

Consequently:

- x is precisely measured for y reasonably close to 1. When y becomes smaller than 0.1 , first the resolution in x rapidly increases to unacceptable values, and second, any miscalibration of the electron energy is amplified in x by this $\frac{1}{y}$ factor, leading to a completely wrong measurement of x.

- Q^2 is very well measured with the possible exception (see below) of very small scattering angles, due to the $\tan\frac{\theta}{2}$term. The influence of energy smearing or energy miscalibration bears little effect on Q^2.

- Both for x and Q^2, the angular precision has an influence only at very low scattering angles ($\theta \geq 170^0$), and only if the angular resolutions, or the angular biases are greater than a few $mrad$.

The values of the x and Q^2 biases and resolutions obtained bin by bin with the simulation described in the next section are displayed in Fig.8a, and are commented upon and compared with the results of the two "combined" methods in section 5.2 .

4.2 Electron simulation

As mentioned in the software section, we went through a detailed simulation of all the particles, including the electron, of the d.i.s. events going through the H1 detector. When however we came to our analysis, we realised that the electron identification was

not yet good enough(we need $\sim$ 99%!), not to bias our cross-section measurement, which is our main goal here. We thus had to rely on a 4-vector smearing for the electron (and only for the electron), which we tried to render as realistic as possible:
- The electron energy was smeared with:

$$\sigma(E)/E = \frac{0.13}{\sqrt{E}} \oplus 0.01$$

- The electron angle was smeared with:

$$\sigma(\theta) = 2\ mrad \ \ (0^0 \leq \theta \leq 170^0)$$

$$\sigma(\theta) = \frac{(176^0 - \theta^0)}{0.75^0} + 2\ mrad \ \ (170^0 \leq \theta \leq 176^0)$$

This is an estimate of the linear angular resolution degradation down to 10 $mrad$ at 176^0, since only one proportional chamber is available at angles larger that 170^0 [8]. The event was rejected for $\theta \geq 176^0$. The effect of cracks crossed by the electron cannot be tested with this much simpler simulation, but we anyway foresee that with real data we can apply fiducial cuts for electrons whose response is corrupted. The effect of electron misidentification remains to be studied. This includes the treatment of photoproduction background events, which have a huge production rate for faking low x,low Q^2 events at high y. The electron results presented here should thus be taken as optimistic.

4.3 Results with the electron only

Considering the subtle edge effects which creep in at very low scattering angle, we restricted the whole study to a minimal Q^2 of 10 GeV^2 implying a scattering angle larger than 6^0. (The extension down to $3GeV^2$ can be found in W.Hildesheim thesis [9]).

Here, unlike in the case of the hadrons, the electron is always in the geometrical acceptance of the detector. Nevertheless, in the major part of the (x, Q^2) plane, the energy of the scattered electron is $30 \pm 1GeV$. There, the smearing of the measured energy easily prevents any precise reconstruction of x.

- Effect of the energy resolution:

Fig.6 displays the influence of the resolution on the measurable area, according to our definitions. In Fig.6a, we took the H1 energy resolution, while in Fig.6b we used the ZEUS one, according to nominal values. With the strong acceptance condition, the H1 area extends down to $y \sim 0.07$ while the ZEUS one is limited to $y \sim 0.13$. With the weak acceptance condition, both resolutions display a similar behaviour, gaining at high x in the high Q^2 region. Before making conclusions, let us include the effect of the miscalibration of the absolute energy scale, and a possible systematic angular shift due to some misalignment.

- Effect of the absolute energy scale miscalibration:

The goal of both experiments is to control the systematic error on the absolute energy at the 1% level for the electromagnetic scale. In the beginning, reaching a value of 2% will already be some success. We simulated the effect of the combination of the two

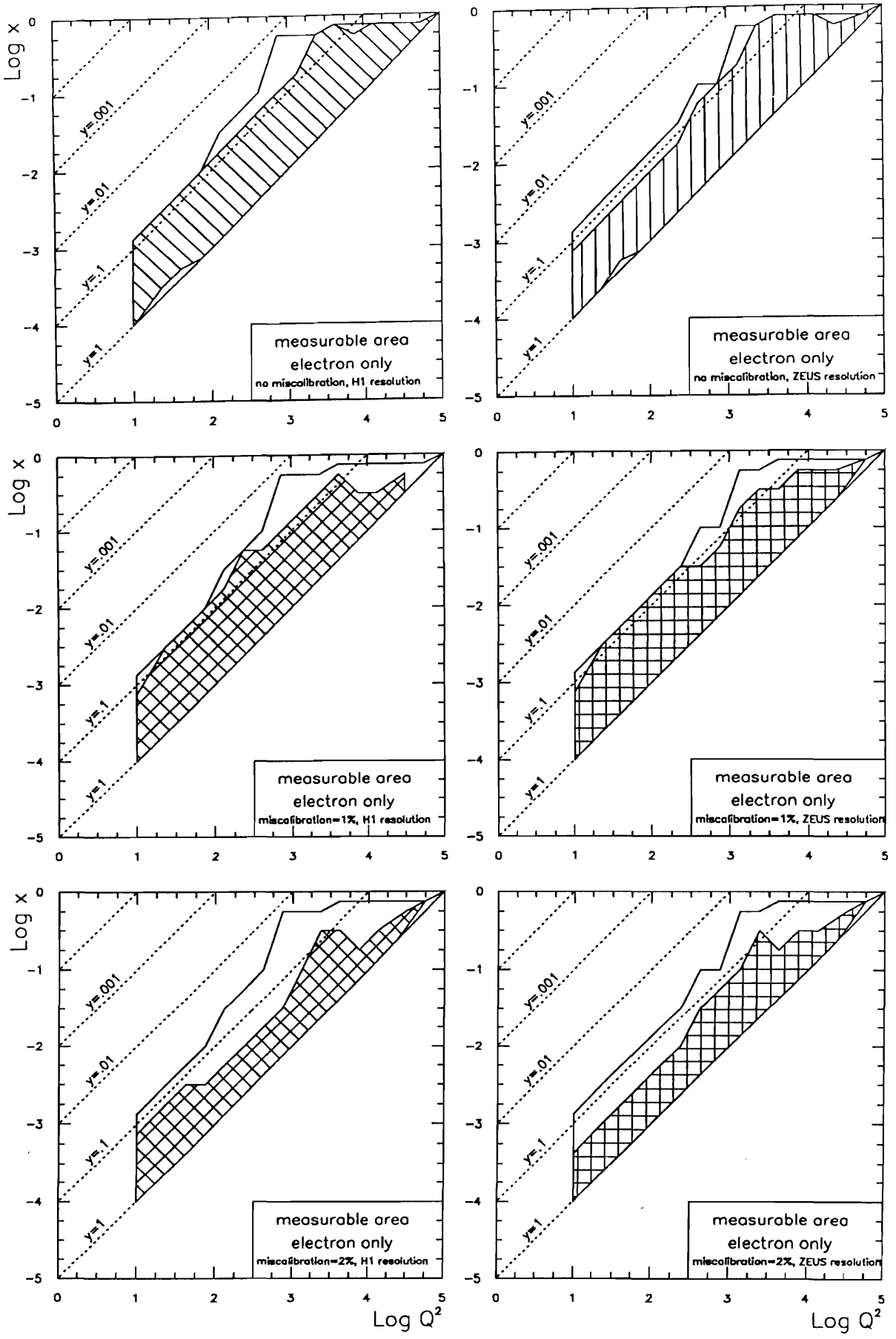

Figure 6 a b c d e f

The largest contour is always the area obtained with the weak smearing condition and no systematics.
In Fig.6a,b the hatched areas are obtained with the strong smearing condition and no systematics.
In Fig.6c–f the hatched regions are the measurable areas taking into account the systematic errors.

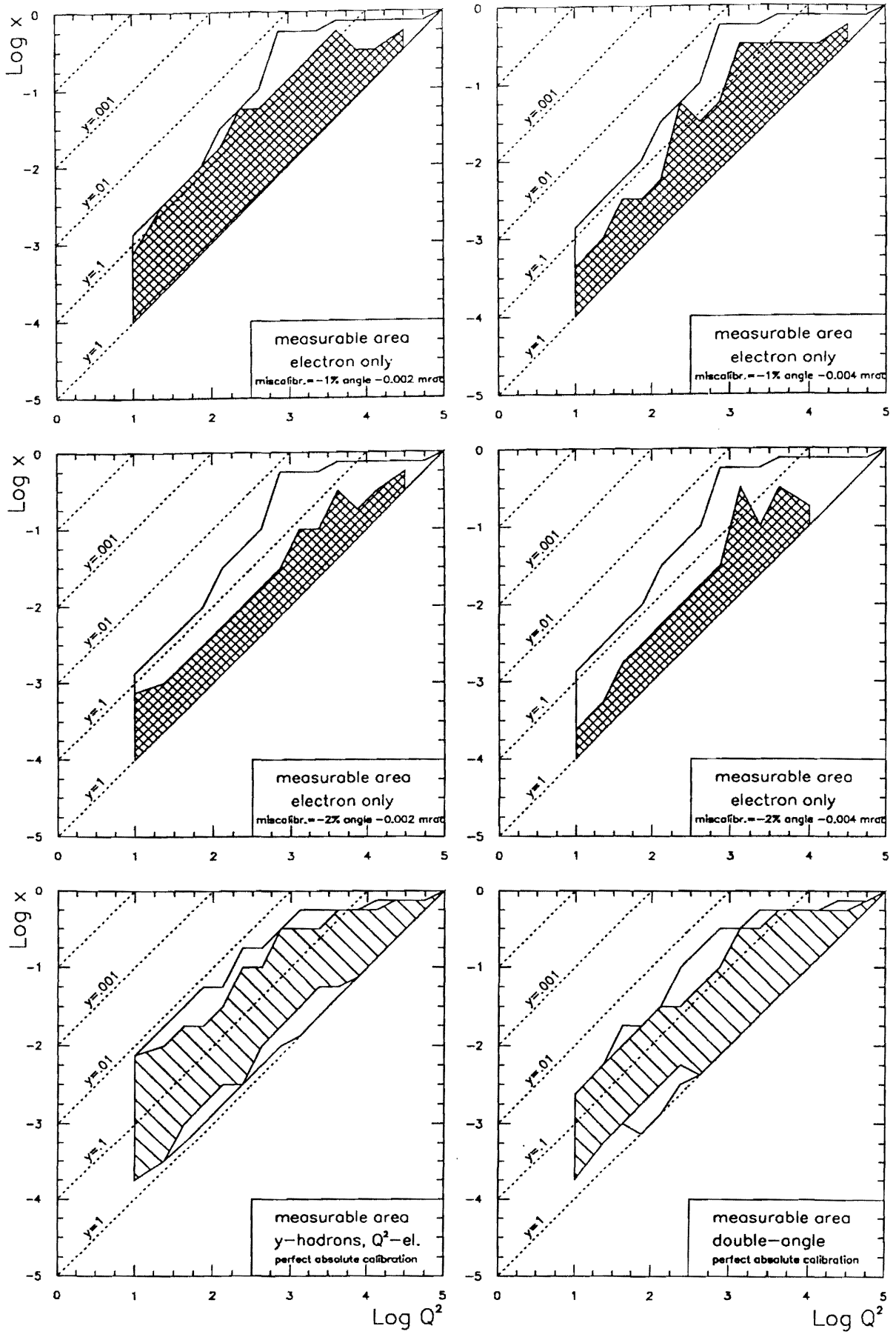

Figure 7 a b c d e f

The largest contour is always the area obtained with the weak smearing condition and no systematics. In Fig.7a−d the hatched regions are the measurable areas taking into account the systematic errors. In Fig.7e,f the hatched areas are obtained with the strong smearing condition and no systematics.

previous resolutions with 4 different values of energy miscalibrations ($\pm 1\%$ and $\pm 2\%$), on the weak acceptance measurable area. The results are displayed in Fig.6c,d,e,f, and the measurable area at say $\pm 1\%$ is the intersection of the two areas obtained when applying separately shifts of $+1\%$ and -1% on the electron energy.
With $\pm 1\%$ miscalibration the measurable area is essentially identical to the initial strong acceptance area. Thus, even with an optimistic energy error the measurable limit is dominated by this systematic error rather than by energy resolution.
This effect is dramatically exhibited with a $\pm 2\%$ miscalibration as we can see in Fig.6e,f. At moderate Q^2 ($\leq 500 GeV^2$) the measurable areas are greatly reduced ($y \geq 0.25$). The shrinkage of the measurable area is enhanced at low Q^2 ($\leq 100 GeV^2$) through combination with a poor energy resolution (ZEUS case, Fig.6f). In the same, physically most interesting region, $H1$ could measure down to $y \geq 0.15$ which appears a tiny difference with the ZEUS limit (0.25). But this represents a large difference in number of events (since it is about the peak of the cross-section), and a reduced number of measurements at a given, low Q^2.

- Effect of an angular misalignment:

We did not study by montecarlo the effect of a *varying* angular resolution, since this effect has been shown before to be tiny, within the expected performances of the trackers of both experiments. All the results presented in this report include the simulation of the expected behaviour of the H1 tracking system, but here we will study the additional effect due to a systematic error on the electron angle. We convoluted this effect firstly with the nominal energy miscalibration ($\pm 1\%$), and then with the realistic one. The results for angular shifts of 2 and 4 *mrad* combined with the two energy miscalibrations are displayed in Fig. 7a,b,c,d assuming the H1 energy resolution in all cases. We can remark that the first,"nominal", case does not display variations. But a 2-*mrad* misalignment combined with a 2% energy miscalibration reduces considerably the measurable area on the whole Q^2 range, and a larger angular shift renders almost impossible a good measurement at low Q^2 with the electron only. These results underline the necessity to control *all* the systematics before being able to provide a cross-section determination.

- Summary on electron systematics:

After combining the effects of some of the several systematic errors expected, we can observe an important reduction of the measurable area, if those are not maintained at their expected low level. It should be emphasized that systematics arising from the electron misidentification, those due to energy tails for electrons close to "cracks", or those involving noise background (both physical and electronical), could not yet been studied. Considering that, we conclude that it will be very difficult to obtain a precise measurement in the early days of HERA, using the electron alone.

5 Cross-sections measurement: e^- and hadrons

5.1 "Mixed" and "double-angle" methods

We already discussed the quality of the y measurement with the hadrons in section 2.1. The determination of Q^2 with the electron is also excellent, since it is based mainly on

the e^- angle determination, except at high y where anyway the dependence to the e^- energy, a well measured quantity in sampling calorimeters, is linear. In the "mixed" method, Q^2 is taken from the electron reconstruction and y from the hadron flow, then:

$$x = \frac{Q_e^2}{s\ y_{JB}}$$

During this workshop, S.Bentvelsen et al.[3] have been through the exercise of estimating which combination of 2 variables among the energies and the angles of the electron and the jet appear the most fruitful, apart from the "electron only", and the jacquet-blondel method: the only serious competitor, which appears on paper surprisingly good, involves simultaneously the angles of the electron and of the jet, and is usually called "double-angle method". The main experimental problem of this method is the definition of an angle of the jet[3][10]. An elegant solution is to make use of the Jacquet-Blondel variables, stripped from their E_e dependence, to extract the "angle" γ of the jet. It is shown in [3] how little bias carry γ with the following definition, even with biased J.-B. variables.

$$\cos\gamma = \frac{(\sum_h p_{xh})^2 + (\sum_h p_{yh})^2 - (\sum_h E - p_{zh})^2}{(\sum_h p_{xh})^2 + (\sum_h p_{yh})^2 + (\sum_h E - p_{zh})^2}$$

We can then make use of the following formulae which are energy independent:

$$Q^2_{\theta\gamma} = 4E_e \frac{\sin\gamma(1+\cos\theta)}{\sin\gamma + \sin\theta - \sin(\theta+\gamma)}$$

$$x_{\theta\gamma} = \frac{E_e}{E_p}\frac{\sin\gamma + \sin\theta + \sin(\theta+\gamma)}{\sin\gamma + \sin\theta - \sin(\theta+\gamma)}$$

$$y_{\theta\gamma} = \frac{\sin\theta(1-\cos\gamma)}{\sin\gamma + \sin\theta - \sin(\theta+\gamma)}$$

5.2 x, Q^2 biases and resolutions

With the combined methods, it becomes difficult to estimate analytically the effect of the various systematics, and we will essentially rely, on the detailed montecarlo for the most complex component, the hadrons, in association with the electron smeared in energy and angle as previously.

We first compared the resolutions and biases of x and Q^2 of these two methods with the "electron only" one. The results, displayed in Fig.8a,b,c, already allow us to guess the extent of the mesurable area:

- the x,Q^2 biases and resolutions obtained with the electron (Fig.8a) are excellent for high y values, as we already saw, but they degrade rapidly when y decreases.

- The "double-angle" (Fig.8c) is very precise in a large area which extends at low $y(\sim 0.02)$, but is plagued by large biases and diverging resolutions at high y (≥ 0.4) for Q^2 up to 500 GeV^2: there, Q^2 becomes badly measured, while in the other two methods, the smearing in Q^2 is always negligible. In the low y region, the measurement is much better than the "electron" one, but the biases are greater than the "mixed" ones.

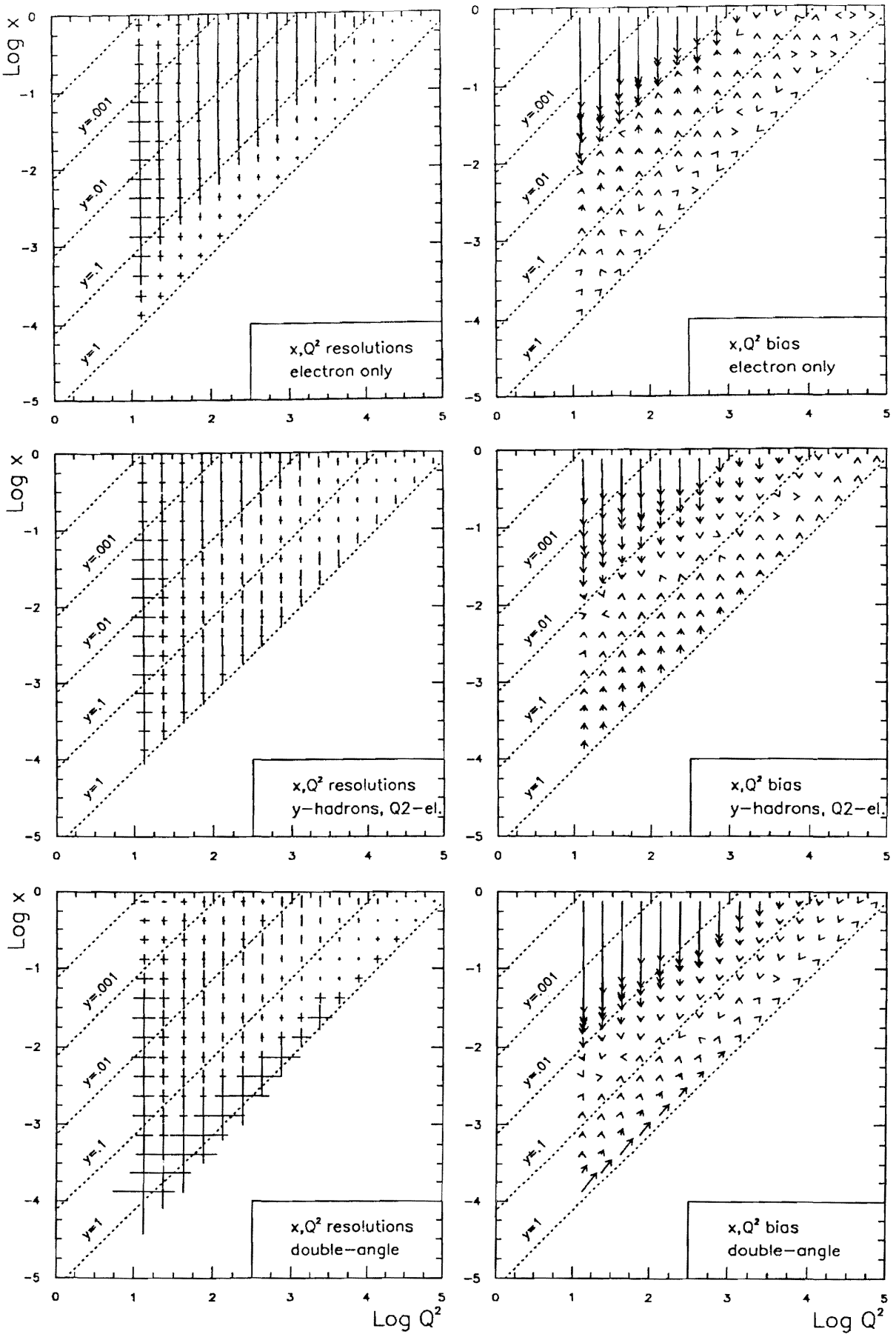

Figure 8 a b c d e f

In the resolutions plots, the error bars display the resolutions of $\Delta x/x$ and $\Delta Q^2/Q^2$: A bar which is one graduation interval long represents a resolution of 25 % . In the plot of the biases, the arrows are drawn between the center of a bin, and the mean value of x and Q^2 reconstructed in this bin.

- In the "mixed" method (Fig.8b) x and Q^2 display acceptable values in the whole area delimited by $y \geq 0.01$. Taking one by one the (x, Q^2) bins of this area, it is worth noting that it is rarely the "best" method, but the one which shows less erratic behaviour.

5.3 Extension of F_2 measurable region

In Fig.7e,f we display for the two combined methods, the areas in which our two smearing conditions are satisfied, assuming a perfect absolute calibration on all particles. We can remark that the "double-angle"method does not extend by much this initial area when we relax the strong smearing condition. This reflects the fact that its biases and resolutions change very abruptly from very good to very poor at some point, contrarily to the "mixed" method which has a much smoother evolution. Both methods give similar results, except for Q^2 lower than $\sim 100 GeV^2$, where the "mixed" method can be measured on two orders of magnitude, while the "double angle" on one only.

- Energy miscalibrations for e^- and hadrons:

A justified worry when combining the lepton with the hadrons, is that one combines not only the advantages but also the inconveniences: the systematic errors.
- The "double-angle" is by construction energy independent, although the determination of the "angle" of the jet is based on hadronic energies.($\cos\gamma$ has only a weak dependence on the energy, since it is a fraction of energies): Thus, miscalibration on the hadronic scale plays a small, indirect role, while errors on the electron side can really be ignored.
- The "mixed" method is directly based on hadronic and leptonic energies. Furthermore, since x is obtained by dividing $Q^2_{e^-}$ by y_{JB}, systematics on the hadronic and electronic energy scales can add up , since they do not necessarily go in the same direction.
Naively we would expect after simulating systematics, a relative stability for the "double-angle" method and a worsening for the "mixed" one, which should vary with the relative directions of hadronic and e^- energy shifts. We thus examined all the following combinations in sytematic energy miscalibrations:

$$e^- : +\varepsilon \text{ , hadrons: } +2\varepsilon$$
$$e^- : +\varepsilon \text{ , hadrons: } -2\varepsilon$$
$$e^- : -\varepsilon \text{ , hadrons: } +2\varepsilon$$
$$e^- : -\varepsilon \text{ , hadrons: } -2\varepsilon$$

for $\varepsilon = 1\%$ (design case) and $\varepsilon = 2\%$ (realistic case)

Empirically, the error on the hadronic scale is roughly twice as bad as what can be achieved with e^-, and these choices are made simply to cover in a few combinations the most significant cases. For all these combinations the results are surprizingly good, even for the "mixed" case: Thus, in Fig.9a,b are displayed for both methods only the worst of the eight previous combinations, which is as expected : e^-: $+2\%$, hadrons: -4% (with no significant difference with $[-2\%,+4\%]$). The "double-angle" measurable area has not changed at all, while the "mixed" method area, shrinks only at high x,high Q^2 ($x \geq 0.3$ and $Q^2 \geq 10^3 GeV^2$). which is a region where we will not see many events in the first years, thus allowing us to work on the calibration!

A posteriori, we can understand the reason why these results are so positive for the "mixed" method: We chose two variables whose systematic shifts depend only

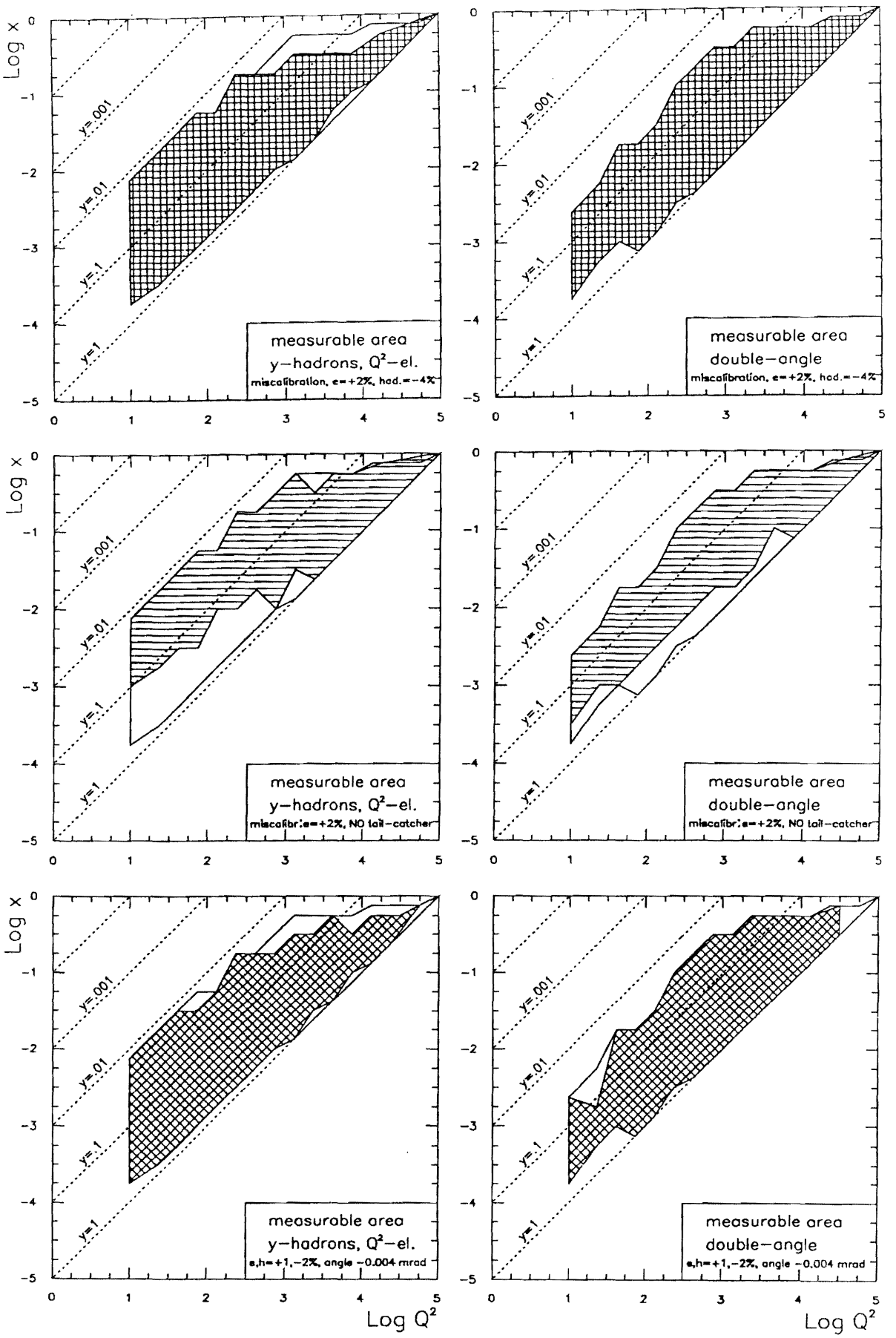

Figure 9 a b c d e f

The largest contour is always the area obtained with the weak smearing condition and no systematics. In Fig.9a–f the hatched regions are the measurable areas taking into account the systematic errors.

linearly with the energy miscalibration.(By opposition for instance with x_e-which has the additional and catastrophic $1/y$ term).
In the worst case above, $\delta x_{mixed} = \delta Q^2 + \delta y = 3\varepsilon$, which remains small enough and, most important, constant over the (x, Q^2) plane.

Before looking at the systematics on the angle, we studied the case in which we would not use at all the Iron tail-catcher. This case is very H1-specific, since then there would be essentially no hadronic coverage in the backward direction ($\theta \geq 135^0$), while ZEUS has an homogeneous calorimeter over $\sim 4\pi$. But it was interesting to test the two methods in this extreme condition. The results are shown in Fig.9c,d. As expected, in both cases the high y region becomes unmeasurable, since most hadrons go in the backward direction in this case. Their detailed behaviour is slightly different: The "double-angle" is unmeasurable on a thin y band extending at high Q^2, while the "mixed", is on a larger y band, but limited at a lower Q^2 case. In both cases the affected region will be measurable with the electron only, and the "new" region which extends down to $y \sim 0.01$ is not contaminated by these losses in the backward region. *En passant*, we can remark some small influence on the high x, high Q^2 region, indicating that the influence of showers leaking outside the main calorimeter is limited to the jets of very high energy.

- Effect of an angular misalignment on combined measurements:

We finally looked at the error introduced by a systematic shift on the electron angle. We added shifts of ± 2 *mrad* and ± 4 *mrad* on top of the nominal energy miscalibration ($\varepsilon = 1\%$). While the first value produces no visible effect, the second one reduces the measurable area of the "double-angle", and most annoyingly at low Q^2 (Fig.9f). We checked that this effect is significant on other combinations of miscalibrations. For the "mixed" method we can also see a small effect, but located at higher Q^2. This confirms that the "double-angle" is not well suited for measurements at $Q^2 \leq 100 - 200 GeV^2$, and that the only potential method to extend them towards lower y is the "mixed" one.

- Remarks on the measurement of the hadronic energy:

In the low Q^2 region, the interesting zone to which one can extend to with the "mixed" method ($0.1 \leq y \leq 0.01$) is populated by events with "current" jets whose low energy will be more difficult to measure than in our simulation which is devoid of electronic noise for instance. Nevertheless, at 30 GeV^2 for example, the energy of the current jet varies between 5 and 20 GeV, and its average angle, between 95^0 and 20^0: the lowest energies are compensated by an ideal angular distribution which favours cross-checks between fully calorimetric measurements and results obtained adding the momentum of charged particles determined with the tracking devices to the neutral particle energies collected in the electromagnetic calorimeters. We are thus confident that at least over 30 GeV^2 our predictions are not too optimistic.

5.4 Modified "mixed" method for treatment of radiative events

Before concluding this survey on systematics, we present here a simple modification of the "mixed" method, to get protected against initial state radiation.

In the expression of both Q^2_{e-} and y_{JB} appears the incident electron energy E_e, whose nominal value is 30 GeV. In case of initial radiation, the photon is lost in the

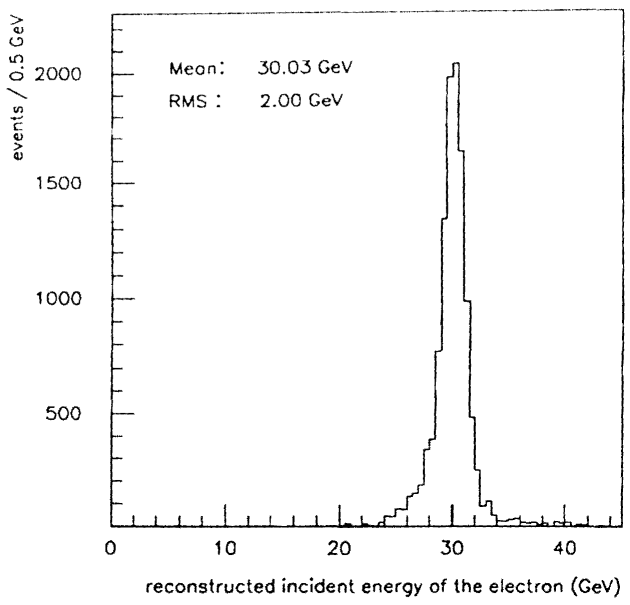

Fig.10a

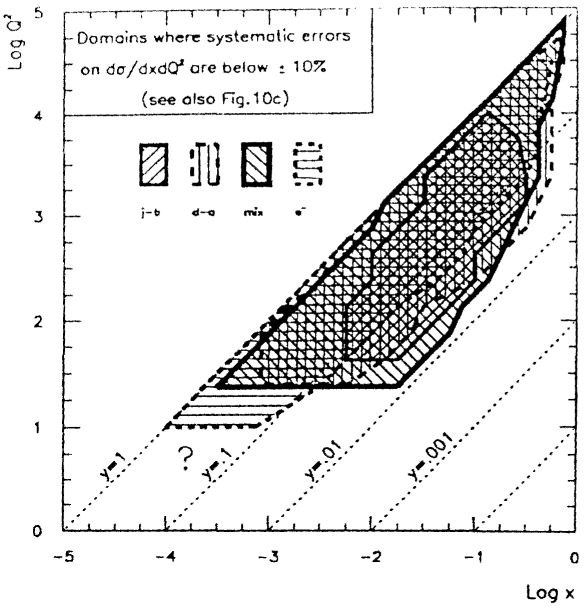

Fig.10b

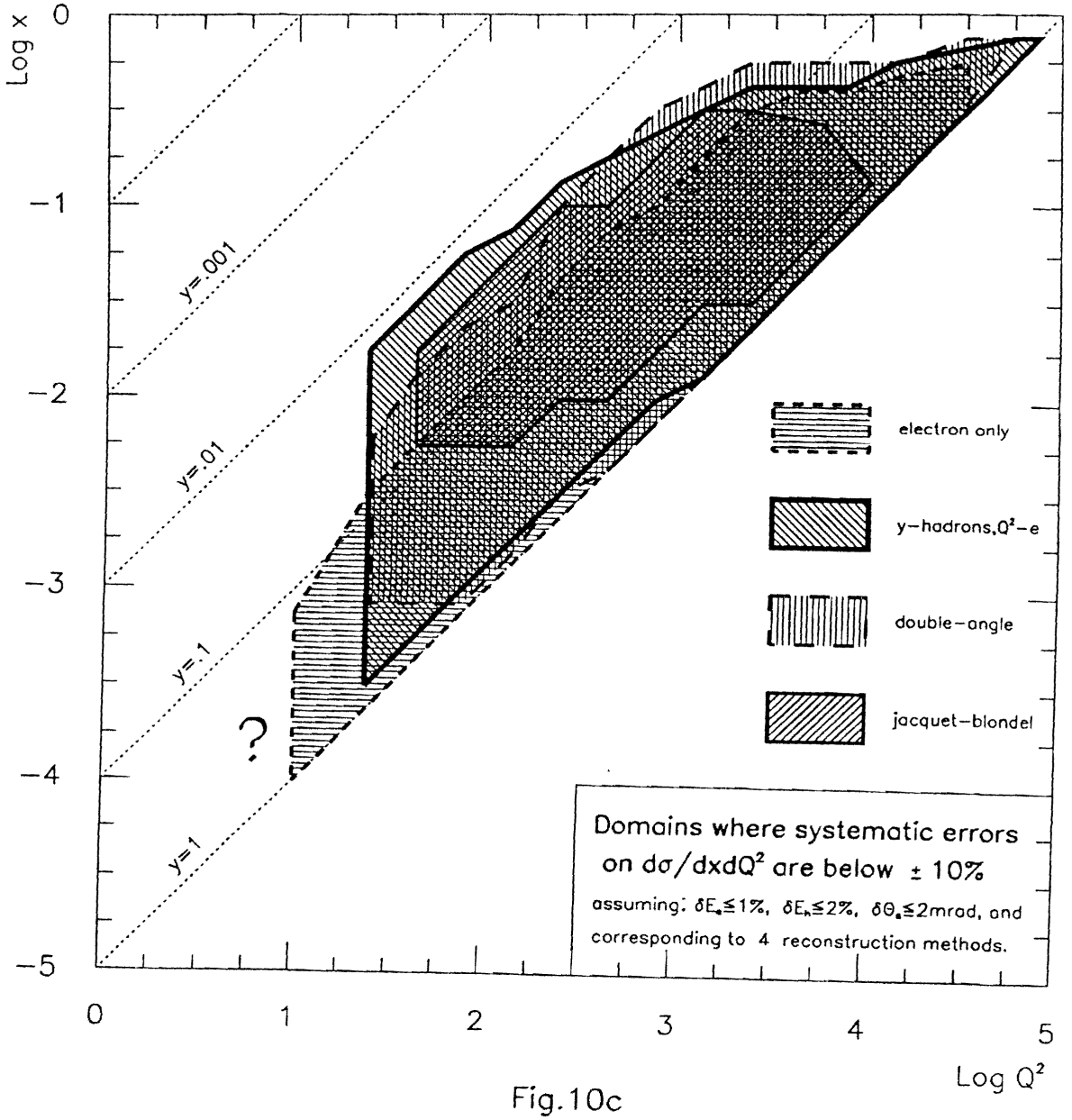

Fig.10c

beam pipe, and E_e becomes smaller. Q^2, x and y can become heavily distorted in case of catastrophic initial radiation if we extract their value using the nominal E_e value. In our overconstrained kinematic system it is possible to extract E_e from the final state variables and making use of γ as defined previously[3]:

$$E_e = E \frac{\sin\theta + \sin\gamma - \sin(\theta+\gamma)}{2\sin\gamma}$$

We studied the accuracy of reconstruction of E_e, on our whole sample of simulated events. The reconstruction does not work well for very high y (≥ 0.7), i.e. in the last bin before the $y = 1$ kinematical limit, but events in that region do migrate towards higher y if we use the correct E_e and thus do not contaminate the rest of the (x, Q^2) plane. Fig.10a show the nice reconstructed spectrum of the incident energy, which ideally would be a monoenergetic peak at 30 GeV since our events were generated without radiative effects. We can also remark that systematic errors behave gently with E_e, since E_e has a simple linear dependence with E[7]. We then modified the "mixed" method in replacing $E_e^{nominal}$ by $E_e^{reconstructed}$ in the expressions of $Q^2_{e^-}$ and y_{JB}, We can see that the systematic error on x and Q^2 due to a miscalibration of the absolute energy of the electron of $\delta E/E = \varepsilon$, changes from :

$$\frac{\delta x}{x} = \varepsilon, \quad \frac{\delta Q^2}{Q^2} = \varepsilon \qquad to \qquad \frac{\delta x}{x} = 2\varepsilon, \quad \frac{\delta Q^2}{Q^2} = 2\varepsilon$$

thus remaining low, of the order of 2 to 4 %.
Finally, we replayed the measurable area game, with this modified mixed method, and we found exactly the same area as before, confirming that the additional systematics are small enough. It remains to be shown that this reconstruction precision is the same for electrons which have actually radiated (smaller E_e), but we can already be confident that we can get rid of the huge discrepancy which appears in the normal "mixed" method, between electron and hadrons measurement, in case of catastrophic initial radiation.

6 Conclusion

We studied the biases of four ways of reconstructing x and Q^2 and their influence on the cross-section determination. We can see in Fig.10c (or, courtesy to our readers who use the "wrong" coordinates system, in Fig.10b with reversed axis) that these methods can be cross-checked in large parts of the (x, Q^2) plane. We will thus be able to measure F_2 in a larger region than what has been calculated before with the two simplest methods, although a (smaller) gap with previous d.i.s measurements will still exist. In the "hatched" areas the cross-section will be measured within $\pm 10\%$ assuming that we will stay within the "design" systematic errors[8]. We stress that to fully benefit from the gain at low Q^2, we need to be able to measure "jets" of very low energy ($\sim 5 - 10$ GeV) a difficult enterprise for the calorimeters of both experiments, which can otherwise be undertaken with a mixed measurement of charged hadrons in the trackers, and neutrals in the calorimeters. Finally to complete this study additional work is needed in many places but in particular on the electron side (better simulation and identification), and on the influence of the overwhelming low Q^2 events.

[7]The sytematic error on θ essentially cancels out.
[8]$\delta E_{e^-} = \pm 1\%$, $\delta E_{had} = \pm 2\%$, and $\delta\theta = \pm 2$ $mrad$.

Acknowledgments

This work could not have taken place without the help of the H1 collaboration, but in particular we want to thank Joel Feltesse for inspiring this work by his 1987 study, and for numerous explanations, Franz Eisele who pushed us in the fruitful direction of the "calibrated energy" option, Stan Bentvelsen and Max Klein for relaxed and useful discussions, and Marie Bernardi for her kindness and patience...

References

[1] H.Abramowicz, K.Charchula, DESY 90-107

[2] J.Feltesse, HERA workshop 87,33

[3] S.Bentvelsen et al., these proceedings.

[4] Study of software compensation for single particles and jets in the H1 calorimeter, H1 calorimeter group, Contributed paper to the XXV International Conference on H.E.P., Singapore 1990.

[5] G.Bernardi, W.Hildesheim, M.Kuhlen, M.Rudowicz, H1 software note-25.

[6] A.Blondel, F.Jacquet, Proceedings of the study of an *ep* facility for Europe, Ed. U.Amaldi, DESY 79/48 (1979), p.391-394.

[7] N.Huot, Ph.D. thesis, University of Paris, 1992, to be published.

[8] Technical Proposal for the H1 detector, H1 collaboration, march,1986

[9] W.Hildesheim, Ph.D. thesis, University of Paris, 1992, to be published.

[10] C.Hoeger, these proceedings.